Distribution patterns of long-runout landslides triggered by the northern Nagano Prefecture earthquake of 2011

Takashi KIMURA[1,*], Kazuhiro HATADA[2], Shin'ya KATSURA[1], Kiyoteru MARUYAMA[1], Kazuya AKIYAMA[1], and Tomoyuki NORO[3]

[1] Snow avalanche and Landslide Research Center, Public Works Research Institute (2-6-8 Nishikicho, Myoko, Niigata 9440051, Japan)

[2] Nippon Koei Co., Ltd. (4-2 Koujimachi, Chiyoda-ku, Tokyo 1020083, Japan)

[3] Research Faculty of Agriculture, Hokkaido University (9-9 Kita-ku, Sapporo, Hokkaido 0608589, Japan)

*Corresponding author. E-mail: t-kimura55@pwri.go.jp

The northern Nagano Prefecture earthquake of 12 March 2011 caused many long-runout landslides. Although the major reason for the long runout is considered to be the abundant snow at the time of the earthquake, other factors that influenced the occurrence and spatial distribution of the long-runout landslides remained unknown. To clarify the primary causes and distribution patterns of the long-runout landslides, this study conducted detailed interpretations of aerial photographs taken on the day of the earthquake and GIS analyses. The results are summarized as follows: 1) The landslides involved two distinct types of movement, slide type and failure type. The failure-type landslides were more likely to travel long distances than were the slide-type landslides. 2) Although about 60% of the failure-type landslides consisted of small-size landslides (i.e., horizontal length of landslide slope <100 m), many of these traveled long distances compared with their slope length. Moreover, the travel distance of the failure-type landslides showed a clear increase tendency as slope length become larger. 3) Despite the similarity in the number of landslides per unit area and in frequency distributions of the slope gradients of hillslopes and landslide slopes between the two studied areas (Sakae-Tsunan and Tokamachi), long-runout landslides were clearly concentrated in the Sakae-Tsunan area, reflecting slope susceptibility to large-scale failure. These results indicate that even within a narrow area in the hanging wall of a seismogenic fault, the occurrence of long-runout landslides can vary depending on mass movement type and landslide size.

Key words: earthquake-triggered landslide, air photo interpretation, travel distance, landslide distribution, snowfall period

1. INTRODUCTION

On 12 March 2011, a strong earthquake (the northern Nagano Prefecture earthquake; M6.7; focal depth of 8 km on a NE–SW trending, NW-dipping reverse fault) struck northern Nagano Prefecture and triggered numerous landslides in mountainous regions of northern Nagano Prefecture and southern Niigata Prefecture. *Has et al.* [2012] found that most of the landslides occurred in the hanging wall of the seismogenic fault, which corresponds to findings from recent reports on distribution patterns of landslides triggered by reverse-fault earthquakes [e.g., *Meunier et al.*, 2007; *Chigira et al.*, 2010; *Hasi et al.*, 2011].

Many long-runout landslides occurred in the hanging wall. Several researchers consider that a major reason for the long runout was the abundance of snow at the time of the earthquake [*Has et al.*, 2012; *Yamasaki et al.*, 2013]. For example, *Yamasaki et al.* [2013] reconstructed the mass movement processes of the Tatsunokuchi landslide, a relatively small landslide (5×10^4 m^3) that traveled a long distance of 795 m from its head scarp, and found that a mass of rock debris that had detached from the slope plunged with very high velocity into abundant snow and mixed with the snow, resulting in the formation of a relatively light-weight and low-friction mass that could travel a long distance. The findings from the Tatsunokuchi landslide indicate that even small landslides have the potential to travel long distances as a result of entrainment of

snow into the displaced mass when they occur during snowfall periods [*Yamasaki et al.*, 2013].

Although a possible mechanism for the movement of long-runout landslides associated with snow has been proposed, the factors that influence the occurrence and spatial distribution of long-runout landslides remain unknown. To clarify the primary causes and distribution patterns of long-runout landslides triggered by the northern Nagano Prefecture earthquake, we compared characteristics of landslide populations between two adjacent areas located in the hanging wall based on interpretations of aerial photographs and GIS analyses.

2. STUDY SITE

A series of high-resolution aerial photographs covering about 200 km^2 of northern Nagano Prefecture and southern Niigata Prefecture was taken on the day of the earthquake (Table 1). In this area, a 73-km^2 study site was established in a mountainous region in the hanging wall (Fig. 1). At the meteorological station nearest the epicenter (JMA Tsunan station: Fig. 1), a 227-cm snow depth was recorded on 12 March 2011. Thus, the slopes of the study site should have been covered by at least 2 m of snow when the earthquake occurred.

The study site was divided along the main ridge line of Higashi-kubiki Hill into the following two areas: the Sakae-Tsunan area (ST; 50 km^2), which includes a southeast-facing slope that forms the left-bank slope of the Chikuma River, and the Tokamachi area (TK; 23 km^2), which includes a northwest-facing slope that surrounds the Koedo and Higashi rivers (Fig. 1). ST consists of Neogene to Quaternary volcanic and sedimentary rocks, whereas TK consists mainly of Neogene sedimentary rocks [*Takeuchi et al.*, 2000].

The distance to the presumed seismogenic fault (Miyanohara fault; Fig. 1) was less than 6.5 km for ST and ranged from 4.2–8.8 km for TK. The landslides triggered by the earthquake were distributed within 18 km of the fault but were concentrated mostly in the hanging wall within 10 km of the fault [*Has et al.*, 2012; *Matsuura et al.*, 2014], a region that included both of these areas.

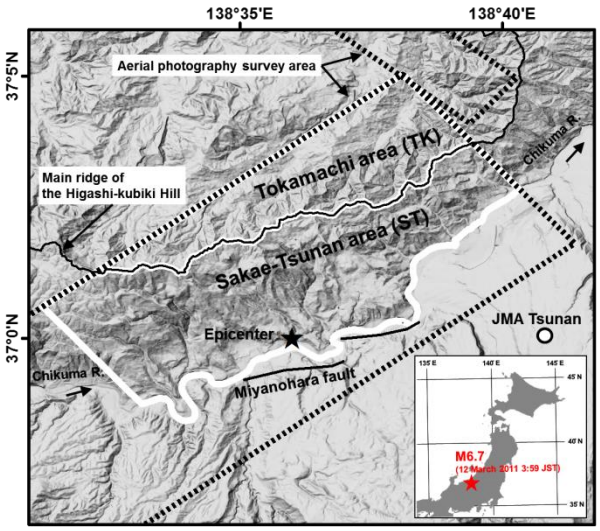

Fig. 1 Map showing the study site and the epicenter of the northern Nagano Prefecture earthquake, 2011. The closest meteorological station (JMA Tsunan) to the epicenter is also shown on the map.

3. METHODS

3.1 Aerial photography interpretations

Landslides triggered by the earthquake were identified easily on the aerial photographs because of the absence of snow cover on their scarp surfaces. For each landslide, the landslide slope and transfer/deposition zone of the displaced mass including snow-mixed debris were delineated on 1:25000-scale topographic maps and manually digitized for GIS analyses.

Previous studies have reported that the earthquake caused several types of landslide movements, such as deep-seated landslide and shallow slope failure movements [*Has et al.*, 2012; *Yamasaki et al.*, 2013; *Matsuura et al.*, 2014]. Because the type of movement is correlated with the velocity and mobility of the landslide [cf. *Cruden and Varnes*, 1996], it is likely to be an important factor determining the travel distance. The high-resolution aerial photographs taken in the area of deep snow cover allowed us to identify the degree of disruption of the mass that occurred in the movement process. Under the deep-snow condition, if a mass slides along the slope without substantial disruption, its main body, covered by a snow layer, remains on the slope. On the other hand, if the mass detached from the slope falls downward, it

Table 1 Summary of aerial photographs used in this study

Date	Flight time	Focal length [mm]	Average flight height above ground level [m]	Ground resolution [m]
12th March 2011	14PM-16PM	120	1,400	0.14

(Note) The aerial photography survey was conducted by Asia Air Survey Co., LTD.

commonly breaks into fragmented debris, so the snow layer is severely disrupted and mixed with debris by the mass movement. Thus, the apparent degree of mass/snow disruption reflects the type of landslide movement.

From this viewpoint, the landslides identified within the study site were classified into two types of movement: slide type, in which the mass with its (partly disrupted) snow layer covered more than 50% of the area of the landslide slope, and failure type, in which the severely disrupted mass and snow layer covers less than 50% of the area of the landslide slope. The method of calculating the ratio of landslide slope area covered by displaced mass (hereafter, mass residual ratio, *MRR*, %) is described in the following section.

3.2 GIS analyses

The horizontal length of the landslide slope (*L*1, m) and the travel distance of the displaced mass (i.e., horizontal length from the lower boundary of the landslide slope to the toe of the mass; *L*2, m) were measured for each landslide. The areas of the landslide slope and the displaced mass were also measured for each landslide. Then, the overlap area between the two was calculated as the *MRR* value. The traveling ratio (*Tr*=*L*2/*L*1: defined by *Usuki et al.*, 2005) was also calculated.

Based on 10-m DEMs provided by the Geospatial Information Authority of Japan, slope gradients for each DEM grid point within the study site and the mean gradient for each landslide slope were calculated.

The measured values were summarized for each area to compare the characteristics of the population of landslides in the two areas. The degree of landslide concentration in each area was evaluated by the landslide number per unit area (*LNA*, slides km^{-2}) and the percentage of area affected by landslides (hereafter, landslide density, %). All analyses were performed using ArcGIS (version 10.2, Esri).

4. RESULTS

4.1 Landslide types and travel distances

According to the results of the air photo interpretations, 82 landslides were identified within the study area (Fig. 2). Among these, 21 landslides (*MRR*s: 52.3–93.7%) were classified as slide type, and the remaining 61 landslides (*MRR*s: 2.3–47.3%) were classified as failure type.

Aerial photographs of six representative landslides are shown in Fig. 3. Three landslides classified as slide type (Fig. 3a–c) involved head scarps and solid masses with a snow layer on their tops. In each of these, the main body of the mass remained on the landslide slope, although the toe of the Kamigo-ueda landslide (Fig. 3b) fluidized and transformed into a channelized flow. The other three

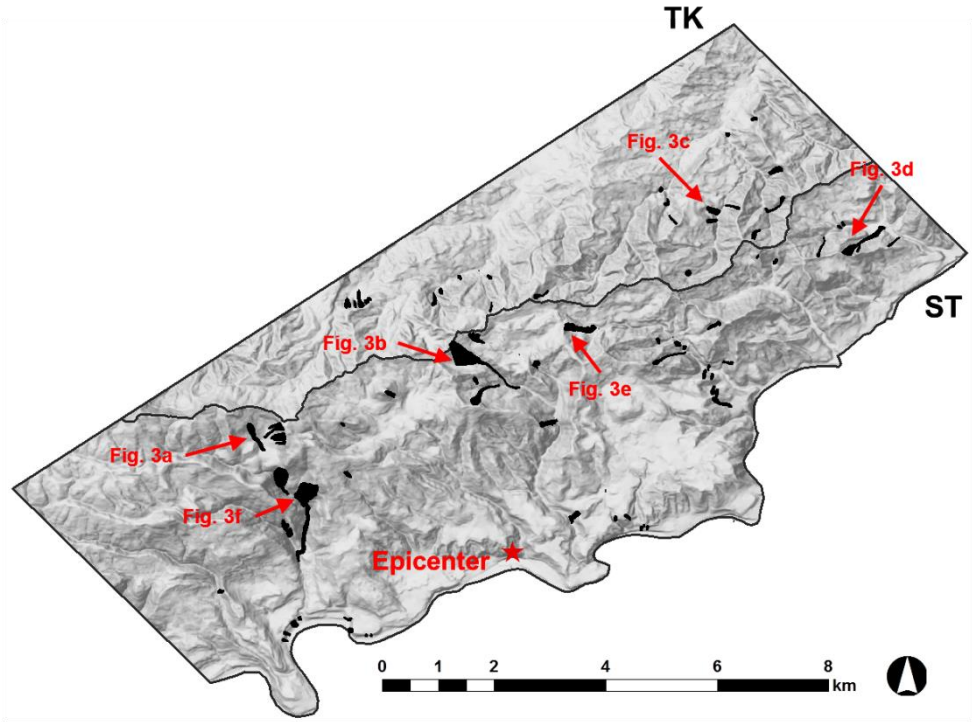

Fig. 2 Shaded relief map showing the location of the 82 landslides identified on the aerial photographs taken on the day of the earthquake. The locations of six landslides in Fig. 3 are indicated by arrows with figure codes.

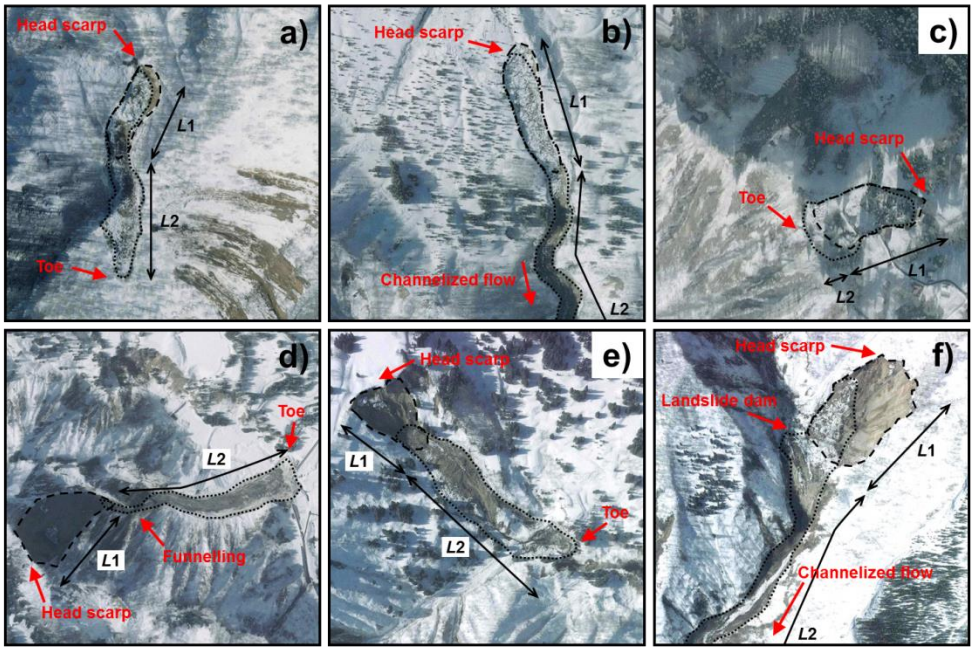

Fig. 3 Aerial photographs of six representative landslides. a) Amamizuyama no.1 landslide; b) Kamigo-ueda no.2 landslide; c) Nakao landslide; d) Tatsunokuchi landslide; e) Taruda landslide; f) Nakajogawa no.1 landslide. The top three landslides (a-c) were classified into slide type, and the bottom three landslides (d-f) were classified into failure type.

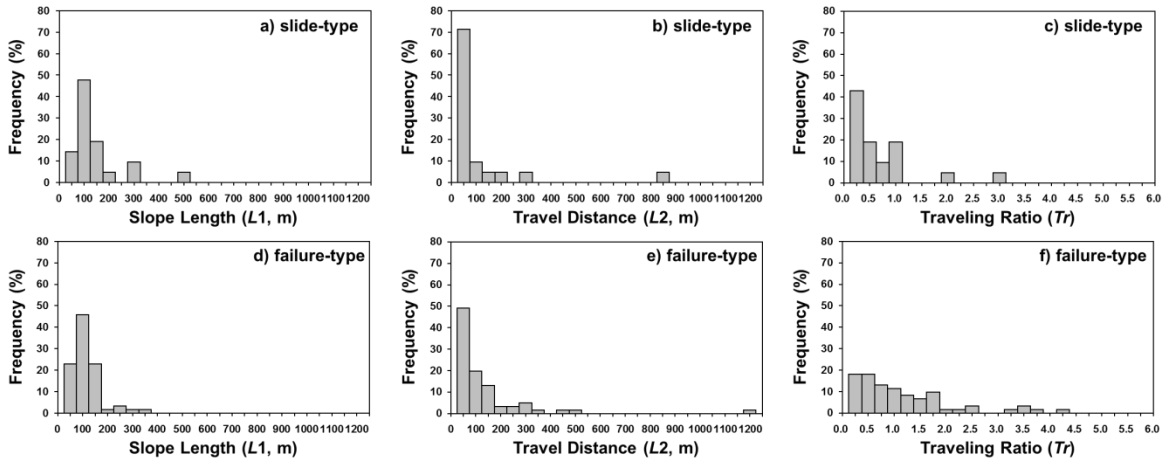

Fig. 4 Frequency distributions of landslide slope length ($L1$), travel distance ($L2$), and traveling ratio (Tr) for each landslide type. Bin widths of the histograms are fixed to 50 m for $L1$ and $L2$ and 0.25 for Tr.

landslides classified as failure-type (Fig. 3d–f) involved exposed rupture surfaces and debris masses that cascaded downslope. The formation of a landslide dam and subsequent occurrence of channelized flow were found at the Nakajogawa no.1 landslide (Fig. 3f).

Frequency distributions of $L1$, $L2$, and Tr for each landslide type are shown in Fig. 4. The size of slide-type landslides ranged in $L1$ from 38 to 496 m and in $L2$ from 2 to 816 m, whereas the size of failure-type landslides ranged in $L1$ from 27 to 333 m and in $L2$ from 2 to 1,153 m. The longest $L2$ in each type occurred for the landslides that transformed into channelized flow (Fig. 3b, f). A common feature between the two types was that about 60% of the landslides had $L1$ <100 m. On the other hand, the ratio of landslides having $L2$ >100 m was 19% for the slide-type population and 31% for the failure-type population. Consequently, the ratio of landslides having Tr >1 was only 9% for the slide-type population but 39% for the failure-type population. The maximum value of Tr was 2.80 in the slide-type population and 4.15 in the failure-type population.

4.2 Characteristics of the landslide population in the two areas

A summary of the landslide population in each of the two areas is shown in Table 2. The *LNA*s of the two areas were similar (1.14 slides km^{-2} in ST and 1.09 slides km^{-2} in TK), but the landslide density in ST (1.37%) was 2.5 times larger than that

Table 2 Summary of the landslide populations in each of the two areas

Area	Area size [km^2]	Landslide number per unit area, *LNA* [slides km^{-2}]	Landslide density [%]	Median size of landslides [a] [m^2]
Sakae-Tsunan (ST)	50	1.14	1.37	3,070 (380－97,180)
Tokamachi (TK)	23	1.09	0.54	2,280 (890－11,380)

[a] Size ranges of the landslides are shown in the parenthesis.

Table 3 Characteristics of movement types and travel distances of the landslide population in each of the two areas

Area	Movement type	Landslide number per unit area, *LNA* [slides km^{-2}]	Travel distance, *L*2		Traveling ratio, *Tr*	
			Range [m]	*L*2 > 100 [a] [%]	Range	*Tr* > 1 [a] [%]
Sakae-Tsunan (ST)	slide	0.22	6－816	36.4	0.01－2.80	18.2
	failure	0.92	2－1,153	30.4	0.04－4.15	39.1
Tokamachi (TK)	slide	0.44	2－94	0.0	0.02－0.81	0.0
	failure	0.65	9－337	33.3	0.14－3.36	40.0

[a] Columns indicate the percentage of the landslides in the population that exceeded a given threshold (i.e., *L*2 = 100 or *Tr* = 1).

in TK (0.54%) due to the difference in landslide sizes. The characteristics of landslide type and travel distance of the landslide populations in the two areas are summarized in Table 3. The *LNA* of slide-type landslides was two times higher in TK (0.44 slides km^{-2}) than in ST (0.22 slides km^{-2}). On the other hand, the *LNA* of failure-type landslides was 1.4 times higher in ST (0.92 slides km^{-2}) than in TK (0.65 slides km^{-2}). The ratio of failure-type landslides having *Tr* >1 was about 40% in both areas, although the maximum value in ST was larger than that in TK. Fig. 5 shows frequency distributions of the slope gradients of hillslopes and landslide slopes in the two areas. In both areas, the slope gradient frequency peaked at 20° for hillslopes and at 30–45° for landslides. These results indicate that ST is more prone to large-scale failure-type landslides, despite similarities in the number per unit area and frequency distribution of slope gradient of landslides in the two areas.

Fig. 6 shows the relationships between *L*1 and *L*2 for the landslides. By focusing on the landslides with *Tr* >1, a clear increase tendency of *L*2 with *L*1 was found for failure-type landslides in ST (Fig 6c), but the relationship was unclear for the other combinations, due mainly to the restriction of size ranges.

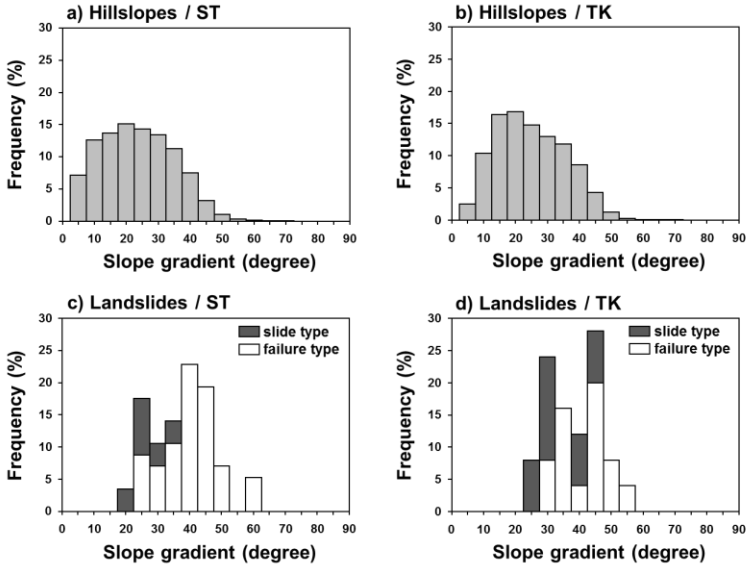

Fig. 5 Frequency distributions of slope gradient of hillslopes and slope gradient of landslide slopes for the two areas. Bin widths of the histograms are fixed to 5 degrees.

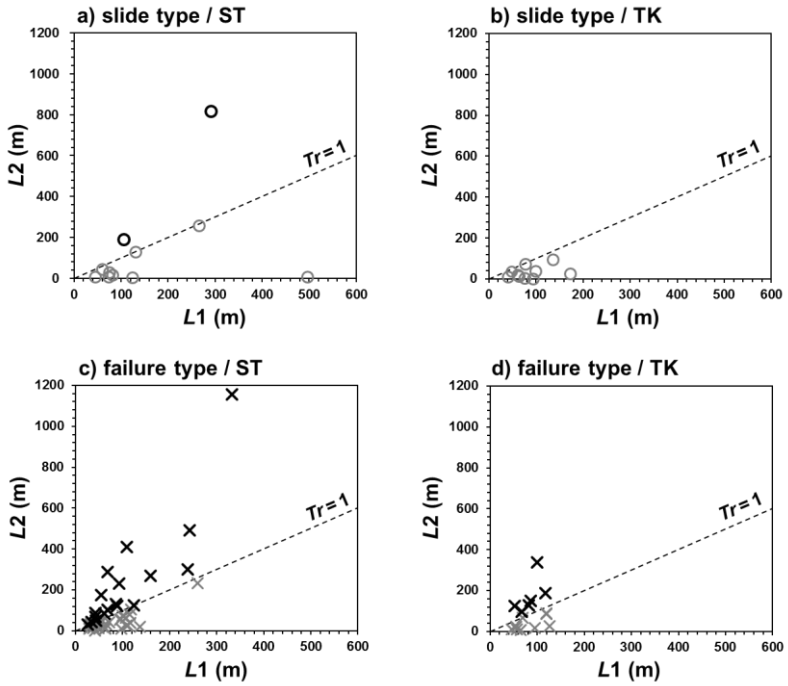

Fig. 6 Relationships between slope length (*L*1) and travel distance (*L*2) of the landslides. Black and grey symbols indicate landslides with traveling ratio (*Tr*) exceeding 1 and less than 1, respectively.

5. DISCUSSION

5.1 Causes of long runout

Landslides with *Tr* >1 accounted for 9% of the slide-type population (max *Tr*: 2.80) and 39% of the failure-type population (max *Tr*: 4.15) (Fig. 4c, f). *Usuki et al.* [2005], who analyzed *Tr* of 109 landslide disasters in Japan triggered by rainfall or snowmelt, reported that the range of *Tr* reached 3.40 and that about 20% of the landslides had *Tr* >1. Comparing our results with those in that report, the frequency distributions of *Tr* for the slide-type population were biased toward short travel distances, whereas those of the failure-type population were biased toward longer travel distances. Thus, failure-type landslides are more prone to travel long distances. *Usuki et al.* [2005] also pointed out that a landslide was more likely to travel a long distance if disruption of its mass became advanced; this corresponds to our results. Moreover, the travel distance of failure-type landslides showed a clear increase tendency with slope length (Fig. 6), suggesting that failure processes and mass volume are the primary causes of long runout.

As *Yamasaki et al.* [2013] demonstrated for the movement processes of the Tatsunokuchi landslide (Fig. 3d), disruption of mass allows landslides to entrain much snow into the mass, resulting in long travel distances. Because about 60% of the failure-type population consisted of landslides having *L*1 <100 m (Fig. 4) and many of these traveled long distances compared with their slope lengths (i.e., *Tr* >1: Fig. 6c, d), processes similar to those occurring in the Tatsunokuchi landslide (*L*1: 243 m) are likely to occur in such small-size landslides.

Although there was much snow around the study site at the time of the earthquake, snowmelt had not yet substantially decreased the snow cover [cf. *Matsuura et al.*, 2014]. For this reason, the soil water content of the hillslopes was considered to be low. Additionally, a dammed lake became apparent behind the debris mass of the Nakajogawa no.1 landslide (Fig. 3f) 7 days after the earthquake occurrence (on 19 March 2011) [*Forestry Department of Nagano Prefectural Government*, 2013], although the drainage area upstream from the landslide dam was 3.4 km^2. This suggests low stream flow at the time of the earthquake. Under such a dry condition, both the entrainment of snow into the displaced mass and the snowmelt water supply available to its movement processes may be crucial for landslide travel distance, even if the mass reaches a stream channel.

Many long-runout landslides triggered by earthquakes have been reported in Japan [e.g., *Ishikawa*, 1999; *Yoshimatsu*, 2000], but there is no record of such landslides during snowfall periods except during the northern Nagano Prefecture earthquake. The western Nagano Prefecture earthquake of 14 September 1984 (M6.8; focal depth of 2 km on a NE–SW-trending right-lateral strike-slip fault) caused markedly severe damage to

lives and property due to the occurrence of long-runout landslides. According to the topographic features of several long-runout landslides described by *Yoshimatsu* [2000], the landslides triggered by the earthquake can be regarded as failure-type landslides (he described the landslides as large-scale slope failures); these landslides had $L1$, $L2$, and Tr ranges of 100 to 800 m, 400 to 10,000 m, and 4.0 to 12.5, respectively. The fact that large-scale slope failures caused long-runout landslides corresponds to our results. However, our results also showed that many small-scale slope failures traveled longer distances compared with their slope lengths (Fig. 6c, d). This tendency could be a characteristic of long-runout landslides affected by snow. To understand how much snow affects landslide runout, future work should compare the size dependence of travel distance of landslides trigged by the northern Nagano Prefecture earthquake with that of those triggered by other earthquakes that occurred during snow-free periods, such as the western Nagano Prefecture earthquake.

Although only a few slide-type landslides traveled a distance longer than the slope length (Table 3, Fig. 6a, b), a distinctive long-runout landslide whose toe (of the mass) transformed into channelized flow was found in ST (the Kamigo-ueda landslide: Fig. 3b). Because slide-type landslides occurred on gentler slopes compared with failure-type landslides (Fig. 5) and the main body of the masses slid while maintaining its structure (Fig. 3a-c), slide-type landslides may initiate as relatively slow mass movements without significant entrainment of snow into the mass. An examination of the processes that transform a solid landslide with relatively slow velocity into a channelized flow is another topic for future work.

5.2 Distribution patterns of long-runout landslides

By comparing the characteristics of the landslide populations in the two adjacent areas, we found that long-runout landslides were concentrated in ST and that both the maximum travel distance and traveling ratio were larger in ST than in TK (Table 3, Fig. 6). The median size of landslides was also larger in ST than in TK (Table 2). Additionally, the number of failure-type landslides, which were more likely to travel longer distances, was higher in ST (Table 3). From these results, it can be concluded that the distribution of the long-runout landslides reflects the susceptibility of the slope to large-scale failure triggered by earthquakes.

Meunier et al. [2007] analyzed regional patterns of landslides caused by three large earthquakes in countries around the Pacific rim and revealed that landslide density, defined as the ratio of the area affected by landslide to the area with local slope greater than 20% within each 5-km-wide window parallel to the seismogenic fault, was greatest in the area of strongest ground acceleration and decayed with distance, suggesting a landslide attenuation law that corresponds to the attenuation of ground acceleration. The regional patterns of landslide density presented by *Meunier et al*. [2007] showed 25–45% decreases from the highest-value areas to adjacent areas (i.e., up to a 10-km separation from the highest-value areas near the seismogenic faults), whereas our results showed a 61% decrease in landslide density within 10 km from the fault (from 1.37% in ST to 0.54% in TK: Fig. 2, Table 2). The sharp decrease in landslide density for the northern Nagano Prefecture earthquake indicates that not only the attenuation of ground acceleration with distance from the fault but also other local factors should be taken into account to explain the pattern of landslide density.

The local amplification of seismic motions associated with slope convexities is one probable factor. This effect causes clustering of earthquake-triggered landslides on steep crest-side slopes [*Meunier et al.*, 2008]. However, the frequency distributions of the slope gradients of hillslopes and landslide slopes were similar for the two areas (Fig. 5). We need to consider additional controlling factors of landslide occurrence (e.g., lithological properties) to derive a reasonable explanation for the sharp decrease in landslide density.

In each type of movement, the landslide that transformed into a channelized flow (Fig. 3b, f) traveled the longest distance. *Ishikawa* [1999] observed topographic features of landslide-initiated debris flows triggered by earthquakes and suggested that fluidization of the displaced mass was the primary cause of transformation to debris flow and the consequent long runout and also that whether the mass fluidized depended strongly on the steepness and flow angle of the headwater channel compared with the landslide slope inclination. Moreover, the authors recently demonstrated that occurrence of long-runout landslides triggered by snowmelt is concentrated on slopes with steep valley topography, such as headwater channels [*Kimura et al.*, accepted]. The similarity of the results in these studies indicates that a consideration of slope and headwater channel topography, where channelized flows are more likely to occur, has a great potential for mitigating landslide disasters, beyond the

difference in triggering mechanism. Further analyses of the long-runout landslides triggered by the northern Nagano Prefecture earthquake will provide a better understanding of the topographic controls on landslide runout.

6. CONCLUSIONS

This study used detailed interpretations of aerial photographs taken on the day of the northern Nagano Prefecture earthquake and GIS analyses to clarify the primary causes and distribution patterns of long-runout landslides triggered by the earthquake, which occurred during a snowfall period. The results are summarized below:

1. The landslides involved two distinctive types of movement: slide type and failure type. The failure-type landslides were more likely to travel a long distance than were the slide-type landslides.
2. About 60% of the failure-type landslides were small-sized landslides (i.e., $L1$ <100 m), and many of these traveled long distances compared with their slope lengths. Moreover, the travel distance of failure-type landslides showed a clear increase tendency as the slope length become larger.
3. Despite similarity in the number of landslides per unit area and frequency distributions of the slope gradients of hillslopes and landslide slopes between the two areas, long-runout landslides were clearly concentrated in ST, reflecting slope susceptibility to large-scale failure.

These results indicate that even within a narrow area in the hanging wall, the occurrence of long-runout landslides can vary depending on mass movement type and landslide size.

ACKNOWLEDGMENT: The authors are grateful to Nagano and Niigata Prefectures, which provided us reports on the sediment-related disasters caused by the earthquake, and also to Dr. Has Baator for providing initial air photo interpretation data and information about the field surveys conducted 2–6 days after the earthquake occurred.

REFERENCES

Chigira, M., Wu, X., Inokuchi, T. and Wang, G. (2010): Landslides induced by the 2008 Wenchuan earthquake, Sichuan, China, Geomorphology, Vol. 118, No. 3, pp. 225-238.

Cruden, D.M. and Varnes, D.J. (1996): Landslide types and processes, In: Turner, A.K. and Schuster, R.L. (eds.), Landslides: Investigation and mitigation, TRB National Research Council Special Report Vol. 247, National Academy Press, Washington D.C., pp. 36–75.

Forestry Department of Nagano Prefectural Government (2013): Large-scale sediment disaster during snowfall season: A landslide in the upstream of Nakajogawa River, Sakae village, triggered by the northern Nagano Prefecture earthquake of 12 March 2011, 60pp (in Japanese†).

Has, B., Noro, T., Maruyama, T., Nakamura, A., Ogawa, K. and Onoda, S. (2012): Characteristics of earthquake-induced landslides in a heavy snowfall region—landslides triggered by the northern Nagano prefecture earthquake, March 12, 2011, Japan, Landslides, Vol. 9, No. 4, pp. 539-546.

Hasi, B., Ishii, Y., Maruyama, T., Terada, H. Suzuki, S. and Nakamura, A. (2011): Distribution and scale of landslides induced by recent reverse-fault earthquakes in Japan, Journal of the Japan Landslide Society, Vol. 48, No. 1, pp. 23-38 (in Japanese with English abstract).

Ishikawa, Y. (1999): Morphological and geological features of debris flows caused by earthquakes, Journal of the Japan Society of Erosion Control Engineering, Vol. 51, No. 5, pp. 35-42 (in Japanese with English abstract).

Kimura, T., Hatada, K., Maruyama, K. and Noro, T. (accepted): A probabilistic approach to predicting landslide runout based on an inventory of snowmelt-induced landslide disasters in Japan, International Journal of Erosion Control Engineering.

Matsuura, S., Chigira, M., Matsushi, Y., and Okamoto, T. (2014): Sediment-related disasters caused by the Nagano-ken Hokubu Earthquake in the heavy snow season, In: Kawase, H. (eds.), Studies on the 2011 Off the Pacific Coast of Tohoku Earthquake, Springer Japan, pp.157-175.

Meunier, P., Hovius, N. and Haines, J.A. (2007): Regional patterns of earthquake-triggered landslides and their relation to ground motion, Geophysical Research Letters, Vol. 34, No. 20, L20408, DOI:10.1029/2007GL031337.

Meunier, P., Hovius, N., and Haines, J.A. (2008): Topographic site effects and the location of earthquake induced landslides, Earth and Planetary Science Letters, Vol. 275, No. 3, pp.221-232.

Takeuchi, K., Yoshikawa, T. and Kamai, T. (2000): Geology of the Matsunoyama Onsen district, with geological sheet map at 1:50,000, Geological Survey of Japan, 76pp (in Japanese with English abstract).

Usuki, N., Tanaka, Y. and Mizuyama, T. (2005): Investigation on the distribution of long travelling landslides, Journal of the Japan Society of Erosion Control Engineering, Vol. 57, No. 5, pp. 47-52 (in Japanese with English abstract).

Yamasaki, S., Nagata, H. and Kawaguchi, T. (2013): Long-traveling landslides in deep snow conditions induced by the 2011 Nagano Prefecture earthquake, Japan, Landslides, Vol. 10, DOI:10.1007/s10346-013-0419-z.

Yoshimatsu, H. (2000): Large-scale landslides in Mt. Ontake, In: Nakamura, H., Tsuchiya, S., Inoue, K. and Ishikawa, Y. (eds.), Erosion control engineering against earthquake disasters, Kokon-shoin, Tokyo, pp. 45-51 (in Japanese†).

† The title or source is a tentative translation by the authors from the original.